

Spiking patterns of a neuron model to stimulus: Rich dynamics and oxygen's role

Chenggui Yao, Zhiwei He, Tadashi Nakano, and Jianwei Shuai

Citation: *Chaos* **28**, 083112 (2018); doi: 10.1063/1.5018707

View online: <https://doi.org/10.1063/1.5018707>

View Table of Contents: <http://aip.scitation.org/toc/cha/28/8>

Published by the [American Institute of Physics](#)

Articles you may be interested in

[Alternating chimeras in networks of ephaptically coupled bursting neurons](#)

Chaos: An Interdisciplinary Journal of Nonlinear Science **28**, 083113 (2018); 10.1063/1.5022612

[Growth rate of modulation instability driven by superregular breathers](#)

Chaos: An Interdisciplinary Journal of Nonlinear Science **28**, 083110 (2018); 10.1063/1.5025632

[The dynamics of knowledge acquisition via self-learning in complex networks](#)

Chaos: An Interdisciplinary Journal of Nonlinear Science **28**, 083106 (2018); 10.1063/1.5027007

[Predicting search time when hunting for multiple moving targets: A recursive harmonic law](#)

Chaos: An Interdisciplinary Journal of Nonlinear Science **28**, 083109 (2018); 10.1063/1.5004730

Chaos

An Interdisciplinary Journal of Nonlinear Science

Fast Track Your Research. *Submit Today!*



Spiking patterns of a neuron model to stimulus: Rich dynamics and oxygen's role

Chenggui Yao,¹ Zhiwei He,¹ Tadashi Nakano,² and Jianwei Shuai^{3,a)}

¹Department of Mathematics, Shaoxing University, Shaoxing 312000, China

²Graduate School of Frontier Biosciences, Osaka University, 1-1 Yamadaoka, Suita, Osaka 565-0871, Japan

³Department of Physics, Xiamen University, Xiamen 361005, People's Republic of China

(Received 8 December 2017; accepted 23 July 2018; published online 16 August 2018)

Neuronal spiking patterns, which are of fundamental importance for the understanding of information processing in neural systems, can be generated in response to different stimuli. We here investigate in detail the stimulus-induced spiking patterns in a biologically plausible neuron model in which the oxygen concentration and the dynamical concentrations of potassium, sodium, and chloride are considered. Various types of spiking patterns can be induced by the different external potassium accumulations in response to the stimulus, including two different types of epileptic seizure (SZ) and spreading depression (SD) states, two different mixed states of SD and SZ, SZ state with multi-burst, and tonic firing behaviors. Interestingly, we show that these rich spiking patterns can also be induced by the current stimulus with a low oxygen concentration. Furthermore, we reveal that the stimulus can induce two different phase transitions from the SD state to the SZ state according to the phase transition theory, which results in the different electrical activities. All these findings may provide insight into information processing in neural systems. *Published by AIP Publishing.* <https://doi.org/10.1063/1.5018707>

The study of dynamics of seizure and spreading depression has attracted attention of researchers due to their significance in the treatment of diseases. We here study the dynamics of seizure and spreading depression in a biologically plausible neuron model in which the oxygen concentration and the dynamical concentrations of potassium, sodium, and chloride are considered. We found that the current stimuli can induce different external potassium accumulations, generating rich spiking patterns, including bursting in two different types of epileptic seizure (SZ) and spreading depression (SD) states, two different mixed states (i.e., the mixed state of SD state with many SZ states and the mixed state of one SZ state following with one SD state), SZ state with multi-bursting, and tonic firing behaviors.

I. INTRODUCTION

The electrophysiology of epileptic seizures (SZ) which are generally deemed to result from synchronous firing of large neuronal populations has been investigated since the early 1930s,^{1,2} and the phenomenon of spreading depression (SD) which is marked by depolarization of neurons was discovered by Leão in the 1940s.³ The dynamics of seizure and spreading depression have been studied in detail by analyzing the electrical activities and the ion concentration changes.^{10–13} It has been reported that extracellular potassium accumulation could play a critical role in seizure development.^{4–6} In addition, a high external or abnormal potassium concentration can also induce hippocampal epileptic activity.⁷ Furthermore,

recent experiments have also pointed out the critical role of a reduction of the $\text{Na}^+ - \text{K}^+$ pump⁸ and impairment of the glial K^+ uptake⁹ in the epileptic activity of neurons.

It is well known that the variation of ion concentrations is closely related to the electrical activity of individual neurons. During the spiking activity of neurons in response to external stimulus, the concentrations of different ions will typically change,¹⁴ especially for extracellular potassium ($[\text{K}^+]_o$), intracellular sodium ($[\text{Na}^+]_i$), and intracellular chloride ($[\text{Cl}^-]_i$). These ion concentrations can also influence the firing response of a neuron to an external current stimulus. Experiments have observed that the external potassium ions accumulate during neuronal firing in response to the external stimulus^{15–17} and that sodium concentrations are altered due to variation in membrane potential.^{18,19} Furthermore, this external potassium accumulation plays an important role in neuronal hyperexcitability and physiological diseases. For example, it has been reported that the abnormal potassium concentration is observed in the pathological states of hypoxia induced spreading depression²⁰ and in diabetes and arrhythmias.^{21–24} Computer simulations^{25–27} have also suggested that the variations in ion concentrations can lead to some particular physiological electrical activities. The changes in $[\text{K}^+]_o$ can modulate bursting frequency and cause multi-stability.^{28,29}

In fact, the microenvironment, such as the cell volume and oxygen concentration, can also play a critical role in neuronal behavior.^{30–32} For example, a change in cell volume, which can be computed during the individual action potentials,^{36,37} can induce a transition in the susceptibility of epileptiform activity.^{33–35} Cell volume changes, which were observed in pathologies including trauma, ischemia, hypoxia, seizures, and spreading depression,^{38,39}

^{a)} Author to whom correspondence should be addressed: jianweishuai@xmu.edu.cn

are important for normal and pathological activities of the brain. It has been found that the spontaneous transition between SZ and SD states occurs as the cell volume increases.⁴⁰ Similarly, the concentration of oxygen has also an intense association with the electrical activity of neurons, and the relationship between them is critical for understanding the basis for normal and pathological brain functions. It is accepted that the structure and function of the brain largely depend on the regular oxygen.^{43,44} For example, a variety of neuronal activities from spikes to seizures and spreading depression are investigated by examining the dynamics as a function of potassium and oxygen.⁴⁰⁻⁴²

In this paper, we investigate the dynamics of seizure and spreading depression in a biologically plausible neuron model with a non-ionic stimulus current. In the model, the dynamic changes of potassium, sodium, and chloride concentrations inside the cell and the oxygen concentration coupled to $\text{Na}^+ - \text{K}^+ - \text{ATP}$ pump activity are considered. Here, we show that various spiking patterns can occur with different stimuli. For direct current injection into the cell, we show that the stimulus can induce rich spiking patterns for low oxygen concentration, including two different types of epileptic seizure (SZ) and spreading depression (SD) states. We further reveal two different transitions between SD and SZ states with the change of direct current strength, which results in different electrical activities. For alternating current, the combined SZ and SD states can manifest two different mixed states (i.e., the mixed state of SD with many SZ states and the mixed state of one SZ followed by one SD state), and a SZ state with many burstings in one stimulus period. The rest of the paper is organized as follows. The neuron model is introduced in Sec. II. Section III is devoted to the numerical results. Finally, conclusions are made in Sec. IV.

II. CELL MODEL

In our work, the membrane potential model which is regulated by ion concentrations via the Nernst equation is a modified model based on the previous work in Ref. 40. In the model, we consider that the cell with radius r_c is surrounded by a shell with radius r_s , and the extracellular shell is a bath with a potassium concentration of 8 mM. The potassium concentration is modulated dynamically by neuron's intrinsic ionic currents, including $\text{Na}^+ - \text{K}^+$ pump current, $\text{K}^+ - \text{Cl}^-$ cotransporter current, the glial buffering current, and the current due to the diffusion of potassium. Furthermore, the effect of oxygen concentration on neural activities is also considered in the model. Here, we set the oxygen concentration as a variable parameter, which is different from Ref. 40 where the oxygen is evolving dynamically.

A. Membrane potential dynamics

For the membrane potential of the cell, we modified the Hodgkin-Huxley formalism by considering the concentration dynamics of sodium, potassium, and chloride ions. The ordinary differential equation governing the membrane potential is as follows:

$$C \frac{dV}{dt} = -(I_{\text{Na}} + I_{\text{K}} + I_{\text{CIL}} + I_{\text{pump}}) + I_{\text{stim}}, \quad (1)$$

where V stands for the membrane potential of the neuron, and the non-ionic stimulus current I_{stim} has an alternating current [AC, $I_{\text{stim}} = A \cos(2\pi \omega t)$] or a direct current (DC, $I_{\text{stim}} = I$). Relevant currents include Na^+ current I_{Na} , K^+ current I_{K} , and chloride (I_{CIL}) leak current. Specifically, somatic currents are given by

$$\begin{aligned} I_{\text{Na}} &= g_{\text{Na}} m^3 h (V - E_{\text{Na}}) + g_{\text{NaL}} (V - E_{\text{Na}}), \\ I_{\text{K}} &= g_{\text{K}} n^4 (V - E_{\text{K}}) + g_{\text{KL}} (V - E_{\text{K}}), \\ I_{\text{CIL}} &= g_{\text{CIL}} (V - E_{\text{CIL}}), \end{aligned} \quad (2)$$

where $E_{\text{K}} = 26.64 \times \ln \left(\frac{[\text{K}^+]_o}{[\text{K}^+]_i} \right)$, $E_{\text{Na}} = 26.64 \times \ln \left(\frac{[\text{Na}^+]_o}{[\text{Na}^+]_i} \right)$, and $E_{\text{CIL}} = 26.64 \times \ln \left(\frac{[\text{Cl}^-]_i}{[\text{Cl}^-]_o} \right)$; $[\cdot]_i$ and $[\cdot]_o$ represent concentrations inside and outside the cell, respectively.

The current I_{pump} is caused by the $\text{Na}^+ - \text{K}^+$ pump which is dependent on ATP, expressed as

$$I_{\text{pump}} = \rho \frac{1}{1 + \exp[(25 - [\text{Na}]_i)/3]} \frac{1}{1 + \exp(8 - [\text{K}]_o)}, \quad (3)$$

where ρ is the pump strength which depends on the oxygen concentration.⁴⁰ To investigate the effect of oxygen, we assume that the concentration of oxygen is a control parameter. With the effect of oxygen in the model, the pump strength $\rho = \rho_{\text{max}} F([\text{O}_2])$ in Eq. (3) is modified according to a sigmoid function of $F([\text{O}_2])$,

$$F([\text{O}_2]) = \frac{1.0}{1.0 + \exp(16 - [\text{O}_2])/4)}, \quad (4)$$

where ρ_{max} is the pump maximal current and $[\text{O}_2]$ is the oxygen concentration.

The currents I_{Na} and I_{K} are controlled by the gating variables m , n , h . The activation and inactivation variables of the sodium current are represented by m and h , respectively, and n is the activation variable of the potassium current. The gating variables h and n satisfy the dynamical equation,

$$\frac{dx}{dt} = \alpha_x(1.0 - x) - \beta_x x, \quad (5)$$

where $\alpha_m = 0.3(V+30)/(1.0 - e^{-(V+30)})$, $\beta_m = 12e^{-(V-55)/18}$, $\alpha_n = 0.03(V+34)/(1 - e^{-(V+34)})$, $\beta_n = 0.375e^{-(V+44)/80}$, $\alpha_h = 0.21e^{-(V+44)/20}$, $\beta_h = 3.0/(1 + e^{-(V+14)})$. We will use the instantaneous steady-state form of m , i.e., $m = \alpha_m/(\alpha_m + \beta_m)$.

B. Ion concentrations dynamics

The intra- and extra-cellular concentrations of K^+ , Na^+ , and Cl^- vary dynamically due to the ion currents. The equations for these ion concentrations are described by

$$\frac{d[\text{K}^+]_o}{dt} = \Gamma_v J_{\text{Kcurrents}} - 2\Gamma_v J_{\text{pump}} - J_{\text{Kglia}} - J_{\text{Kdiff}} + \Gamma_v J_{\text{KCC}}, \quad (6a)$$

$$\frac{d[\text{Na}^+]_i}{dt} = J_{\text{Nacurrents}} - 3J_{\text{pump}}, \quad (6b)$$

$$\frac{d[\text{Cl}^-]_i}{dt} = J_{\text{Clcurrents}} - J_{\text{KCC}}, \quad (6c)$$

where the factor r_v is the cell to shell volume ratio. In the equations above, $J_{K\text{currents}}$ (or $J_{Na\text{currents}}$) denotes ion fluxes caused by potassium currents I_K (or sodium currents I_{Na}) and J_{pump} is the activity of the pump exchanging K^+ or Na^+ . $J_{K\text{diff}}$ is the diffusion of potassium to the bath, and $J_{K\text{glia}}$ and J_{KCC} correspond to glial buffering and $K^+ - Cl^-$ cotransporters, respectively. The expressions for the fluxes are given by

$$\begin{aligned} J_{K\text{currents}} &= \frac{I_K \times r_{av} \times 10^{-3}}{F}, \\ J_{\text{pump}} &= \frac{I_{\text{pump}} \times r_{av} \times 10^{-3}}{F}, \\ J_{K\text{glia}} &= \frac{F(O_2)B_{\text{glia}} \times 10^{-3}}{1 + \exp(18 - [K]_o)/2.5}, \\ J_{K\text{diff}} &= \frac{F(O_2)([K^+]_o - [K^+]_{\text{bath}}) \times 10^{-3}}{\tau_{Kbs}}, \\ J_{Na\text{currents}} &= \frac{I_{Na} \times r_{av} \times 10^{-3}}{F}, \\ J_{KCC} &= \frac{\rho_{KCC} \times 10^{-3}}{r_v} \ln \left(\frac{[K]_i [Cl]_i}{[K]_o [Cl]_o} \right), \\ J_{Cl\text{currents}} &= \frac{I_{CIL} \times r_{av} \times 10^{-3}}{F}, \end{aligned} \quad (7)$$

where r_{av} and F represent the ratio between area and volume of cell and Faraday constant, respectively. B_{glia} and τ_{Kbs} are buffering strength and K^+ diffusion time constant, respectively. ρ_{KCC} is the maximum strength of $K^+ - Cl^-$ cotransporters. Three conservation assumptions are given for the intracellular potassium and extracellular sodium and chloride concentrations: (1) The total amount of sodium is constant; (2) the exchange between extracellular sodium and intercellular potassium is conserved; and (3) the charge due to $[Na^+]$, $[K^+]$, and $[Ca^{2+}]$ ions is conserved.⁴⁰ Thus, the intracellular potassium ($[K^+]_i$) and extracellular sodium ($[Na^+]_o$), chloride concentrations ($[Cl^-]_o$) satisfy the following equations:

$$\begin{aligned} [Na^+]_o &= 144 \text{ mM} - r_v([Na^+]_i - 18 \text{ mM}), \\ [K^+]_i &= 144 \text{ mM} + (18 \text{ mM} - [Na^+]_i), \\ [Cl^-]_o &= [Na^+]_o + [K^+]_o + 2.0[Ca^{2+}]_o, \end{aligned} \quad (8)$$

where $[Ca^{2+}]_o = 1 \text{ mM}$ is the extracellular calcium concentration. The description and values of parameters used in the model are given in Table I. For the computer simulation, the standard fourth-order Runge-Kutta approach with a fixed time step $\Delta t = 0.01$ is applied.

III. RESULTS

A. Two different transitions between SD and SZ states

In our work, we begin with an observation of the spreading depression (SD) and epileptic seizure (SZ) states where the high-frequency bursts are induced by ion concentrations, as shown in Ref. 40. In our simulation with the model, we observe that the oxygen concentration plays a critical role in SD and SZ states. Figure 1 gives the bifurcation for $[K]_o$ as a function of r_c without stimulus. $[K]_o$ always remains in the steady state for low oxygen concentration ($[O_2] < 18.3 \text{ mg/l}$).

TABLE I. Parameter values.

Parameter	Description	Value
r_c	Radius of cell	4.6–4.95 μm
r_s	Radius of the spherical shell	5.0 μm
V_c	Volume of cell	$4\pi r_c^3/3 \mu\text{m}^3$
r_{av}	The ratio between area and volume of cell	$\frac{3}{r_c}$
V_s	Volume of the spherical shell	$4\pi r_s^3/3 \mu\text{m}^3$
r_v	$r_v = \frac{V_c}{V_s}$ volume ratio of cell to shell	0.78–0.97
F	Faraday's constant	96485 C/mol
C	Cell capacitance	1.0 $\mu\text{F}/\text{cm}^2$
g_{Na}	Na^+ conductance	100.0 mS/cm ²
g_K	K^+ conductance	40.0 mS/cm ²
g_{CIL}	Soma Cl^- leakage conductance	0.05 mS/cm ²
g_{KL}	Soma K^+ leakage conductance	0.05 mS/cm ²
g_{NaL}	Soma Na^+ leakage conductance	0.02 mS/cm ²
ρ_{max}	Pump maximal current	3.85 $\mu\text{A}/\text{cm}^2$
$[K^+]_{\text{bath}}$	Potassium concentration in the bath	8.0 mM
$[B]_{\text{glia}}$	Maximal strength of glia uptake	5 mM/s
τ_{Kbs}	K^+ diffusion time constant	0.8 s
ρ_{KCC}	The maximal strength of $K^+ - Cl^-$ cotransporter	0.5 mM/s
O_2	The oxygen concentration of intra cell	10–30 mg/l
A	The amplitude of non-ionic alternating current	$\mu\text{A}/\text{cm}^2$
ω	The angular frequency of non-ionic alternating current	0.008–0.477 Hz
I	The strength of non-ionic direct current	$\mu\text{A}/\text{cm}^2$

For the medium oxygen concentration (18.3 mg/l $< [O]_2 < 18.6 \text{ mg/l}$), we can only observe the SD state in which the cell shows burst-spiking with decreasing amplitude of spikes within a burst.⁴⁰ While both the SD state and the SZ state where the cell shows burst-spiking with almost the same spiking amplitude occur at high oxygen concentration ($[O]_2 > 18.6 \text{ mg/l}$), which is similar to the results of volume-induced transition between SZ and SD states in Ref. 40.

Next, we investigate the effect of the direct current I on the transition between SD and SZ states. Figures 2(a)–2(d)

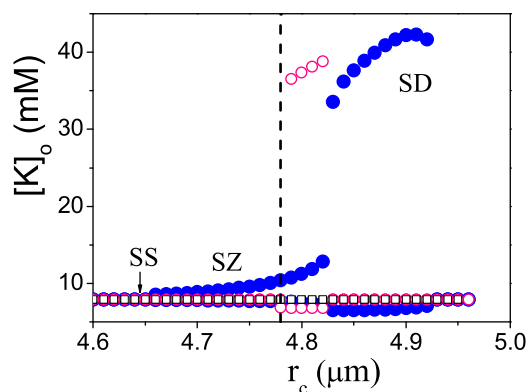


FIG. 1. Bifurcation diagram of $[K]_o$ as a function of r_c for the different oxygen concentrations $[O]_2 = 12.5 \text{ mg/l}$ (black squares), 18.3 mg/l (solid blue circles), and 30.0 mg/l (hollow red circles). The letters SS, SZ, and SD stand for the steady state, epileptic seizure, and spreading depression, respectively.

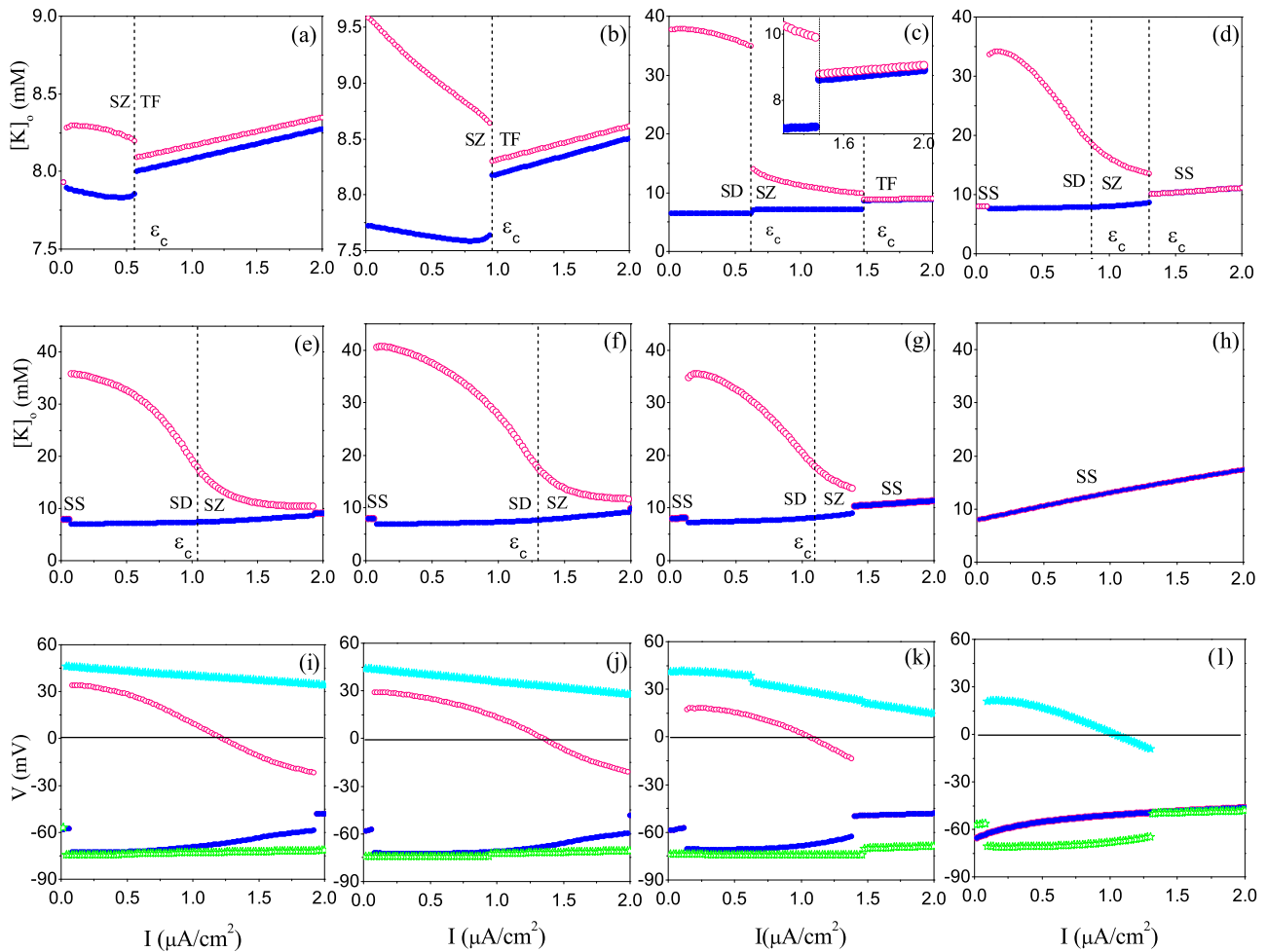


FIG. 2. [(a)–(h)] Bifurcation of $[K]_0$ for the maximal (hollow red circles) and minimal (solid blue circles) values for different parameter values of $[O_2]$ and r_c . From the top row to the middle row, $[O_2] = 30.0 \text{ mg/l}$ and 12.5 mg/l , respectively. From the left-hand column to the right-hand, $r_c = 4.6 \mu\text{m}$, $4.75 \mu\text{m}$, $4.85 \mu\text{m}$, and $4.95 \mu\text{m}$, respectively. [(i)–(l)] Bifurcation of V for the maximal and minimal values for $r_c = 4.6 \mu\text{m}$, $4.75 \mu\text{m}$, $4.85 \mu\text{m}$, and $4.95 \mu\text{m}$, respectively. The stars and circles correspond to $[O_2] = 30.0 \text{ mg/l}$ and 12.5 mg/l , respectively.

give the maximal and minimal values of $[K]_0$ against the strength of current I with high oxygen concentration ($[O_2] = 30 \text{ mg/l}$) for $r_c = 4.6 \mu\text{m}$, $4.75 \mu\text{m}$, $4.85 \mu\text{m}$, and $4.95 \mu\text{m}$, respectively. From Fig. 2, we found that the external potassium concentration has different responses to the stimuli for different sizes. For small radius, the cell is in steady state without stimulus. $[K]_0$ oscillates periodically with a small amplitude for a very small stimulus ($I > 0.02 \mu\text{A}/\text{cm}^2$), and the SZ state can be observed. There is a sudden decrease in the amplitude of $[K]_0$ oscillations when the strength of stimulus increases over a critical value [Fig. 2(a)]. Furthermore, we have checked whether there is bistable state or not. We run the Fortran program with 4000 randomly generated initial conditions ($V_0 \in [-80, 40]$, $n_0 \in [0, 1]$, $h_0 \in [0, 1]$, $K_0 \in [0, 30]$, $Na_0 \in [0, 30]$, and $Cl_0 \in [0, 20]$) for $r_c = 4.6$, $I = 0.3$ and $[O_2] = 30.0 \text{ mg/l}$ and with the simulation time as long as 5000 s. Only the SZ state is observed. We could not find any stable steady state.

A similar phenomenon occurs when the cell is in the SZ state with a medium radius [Fig. 2(b)]. For a large radius, the cell is in the SD state. Then, we found that the direct current can also induce transition from the SD state to the SZ state. $[K]_0$ enters the periodic state with a small amplitude with

increasing I [Fig. 2(c)]. It is similar to the volume-induced transition between SD and SZ states where there is a sudden increase in the amplitude of $[K]_0$.⁴⁰ We suggest that this transition is the first order phase transition according to the theory of transition. With the largest radius tested, the cell is in steady state, the second phase transition from the SD state to the SZ state can also be observed in Fig. 2(d) where the maximal values of $[K]_0$ decrease continuously with increasing I .

The current-induced second order phase transition can also be observed for the low oxygen concentration ($[O_2] = 12.5 \text{ mg/l}$) for $r_c = 4.6 \mu\text{m}$, $4.75 \mu\text{m}$ and $4.85 \mu\text{m}$ which are shown in Figs. 2(e)–2(g). As we are interested in the relationship between the phase transition and electrical activities, Figs. 2(i)–2(l) show the maximal and minimal values of V as a function of I for $[O_2] = 30 \text{ mg/l}$ and 12.5 mg/l with $r_c = 4.6 \mu\text{m}$, $4.75 \mu\text{m}$, $4.85 \mu\text{m}$, and $4.95 \mu\text{m}$, respectively. Comparing Figs. 2(d)–2(g) with Figs. 2(i)–2(l), we found that the maximal potential V decreases continuously below zero when the maximal values of $[K]_0$ decrease continuously with increasing I , while the value of the maximal potential V is always beyond 15 mV when the maximal values of $[K]_0$ vary discontinuously. As a result, the different phase transitions can account for the different electrical activities.

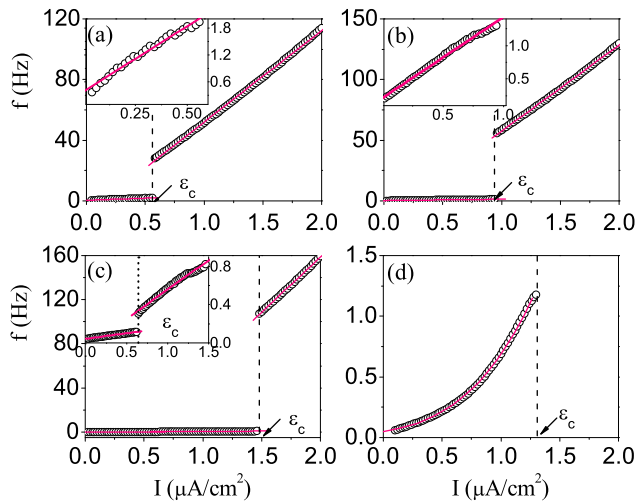


FIG. 3. [(a)–(d)] The average output frequency f as a function of I with $[O_2] = 30.0 \text{ mg/l}$ for $r_c = 4.6 \mu\text{m}$, $4.75 \mu\text{m}$, $4.85 \mu\text{m}$, and $4.95 \mu\text{m}$, respectively. The insets of (a), (b), and (c) show a zoomed-in part near the critical transitions of (a), (b), and (c), respectively. The red lines stand for the fitted curves.

Figures 3(a)–3(d) show the average oscillation frequency f of $[K]_o$ as a function of I with $[O_2] = 30 \text{ mg/l}$ for $r_c = 4.6 \mu\text{m}$, $4.75 \mu\text{m}$, $4.85 \mu\text{m}$, and $4.95 \mu\text{m}$, respectively. We found that the response of oscillation frequency to the stimulus is also different for the different radii. The frequency increases with an increase in I . However, the frequency depends discontinuously on the strength of stimulus when the radius is less than the critical value $r_c < r_{cc}$ ($r_{cc} = 4.915 \mu\text{m}$) [Figs. 3(a)–3(c)]. On the other hand, the frequency increases continuously with an increase in I when $r_c \geq r_{cc}$ [Fig. 3(d)]. Our numerical experiments show that, if $r_c < r_{cc}$, the oscillation frequency of $[K]_o$ is piecewisely linear with I ; otherwise, it is a continuous function of I .

To show spiking activities clearly, we plot the time series of V and $[K]_o$ in Figs. 4(a)–4(e) at $r_c = 4.95$ and $I = 0.3 \mu\text{A/cm}^2$ (a), $r_c = 4.95$ and $I = 1.1 \mu\text{A/cm}^2$ (b), $r_c = 4.85$ and $I = 1.0 \mu\text{A/cm}^2$ (c), $r_c = 4.85$ and $0.3 \mu\text{A/cm}^2$ (d), and $r_c = 4.85$ and $0.6 \mu\text{A/cm}^2$ (e), respectively. From Fig. 4, we found that the different $[K]_o$ accumulations lead to the different spiking activities. Figure 4(a) gives SD bursting, and $[K]_o$ oscillates periodically with a very large amplitude. Figure 4(b) is devoted to an example of the SZ bursting, and the amplitude of $[K]_o$ is small. Compared with Fig. 4(b), however, Fig. 4(c) shows a different SZ state which has the higher potential. Figure 4(d) presents a special SD state which is similar with the mixed state with SZ and SD states in Ref. 40. Figure 4(e) gives the tonic firing state (TF) with a high frequency, and $[K]_o$ fluctuates periodically with a very small amplitude.

To obtain a global view, the dynamical phase diagram on the $([O_2], I)$ plane is shown in Fig. 5. The response of cell to the direct current exhibits five primary features: steady state (SS), SZ_1 and SZ_2 state, SD state, and TF state. The gray, blue, cyan, pink, and orange regions correspond to SS, SZ_1 , SZ_2 , SD, and TF state in Fig. 5, respectively. The SZ_1 and SZ_2 are two different kinds of SZ states. The SZ_1 and SZ_2 states are determined by the maximal value of $V > 0.0 \text{ mV}$ and $V < 0.0 \text{ mV}$, respectively. From these figures, we found

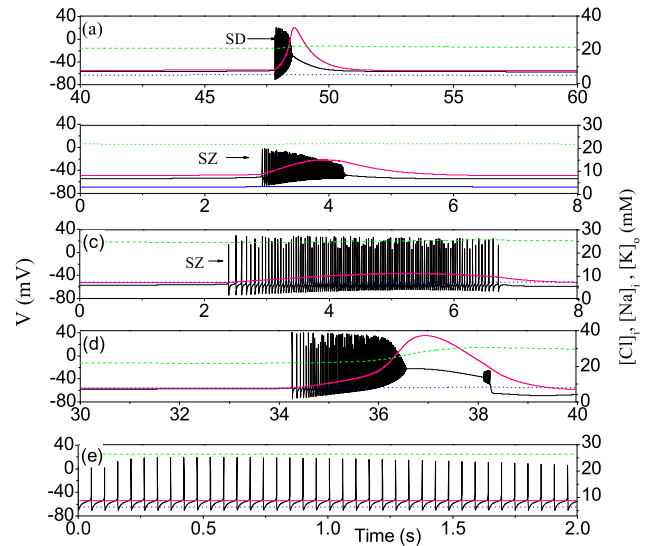


FIG. 4. Time series of V (black lines), $[K]_o$ (pink lines), $[Na]_i$ (green lines), and $[Cl]_i$ (blue lines) for $r_c = 4.95$ and $I = 0.3 \mu\text{A/cm}^2$, giving a single SD event (a), $r_c = 4.95$ and $I = 1.1 \mu\text{A/cm}^2$, giving a single SZ event with low amplitude spiking (b), $r_c = 4.85$ and $I = 1.0 \mu\text{A/cm}^2$, giving a SZ event with high amplitude spiking (c), $r_c = 4.85$ and $0.3 \mu\text{A/cm}^2$, giving a special SD state (d), and $r_c = 4.85$ and $0.6 \mu\text{A/cm}^2$, giving a tonic firing state (e).

that the direct current can induce SD, SZ_1 , and SZ_2 states at the low oxygen concentration ($[O_2] < 18.3 \text{ mg/l}$) with which the cell always remains in the steady state without stimulus [Figs. 5(a)–5(c)]. Furthermore, we can observe that the low oxygen concentration can generate the SD state more readily.

B. The rich bursting activities with spreading depression and epileptic seizure

In order to gain more insight into the role of stimulus on spiking patterns of cell, we turn to investigate the effect

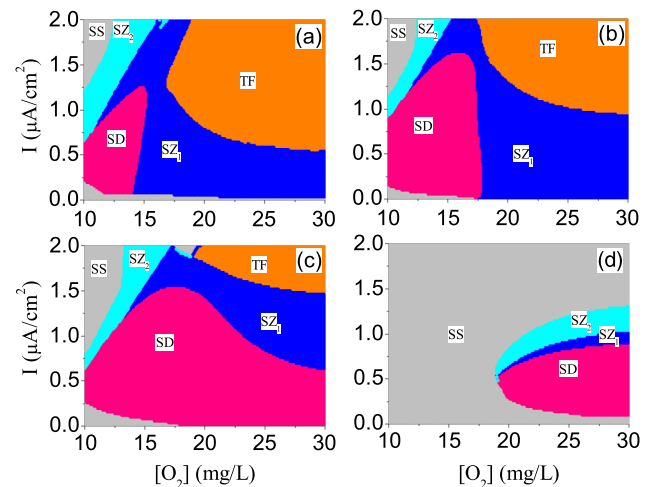


FIG. 5. [(a)–(d)] Phase diagram on the $([O_2], I)$ plane for different dynamical regions for $r_c = 4.6 \mu\text{m}$, $4.75 \mu\text{m}$, $4.85 \mu\text{m}$, and $4.95 \mu\text{m}$, respectively. The letters SS and TF stand for the steady state and tonic firing state where the cell shows spike with a high frequency. The letters SZ_1 and SZ_2 correspond to epileptic seizure with high and low potential, respectively. The SD and SZ states are determined by the maximal value of $[K]_o > 20 \text{ mM}$ and $[K]_o < 20 \text{ mM}$, respectively. The SZ_1 and SZ_2 states are determined by the maximal value of $V > 0.0 \text{ mV}$ and $V < 0.0 \text{ mV}$, respectively. The TF state is determined by the spiking (not bursting) of neuron.

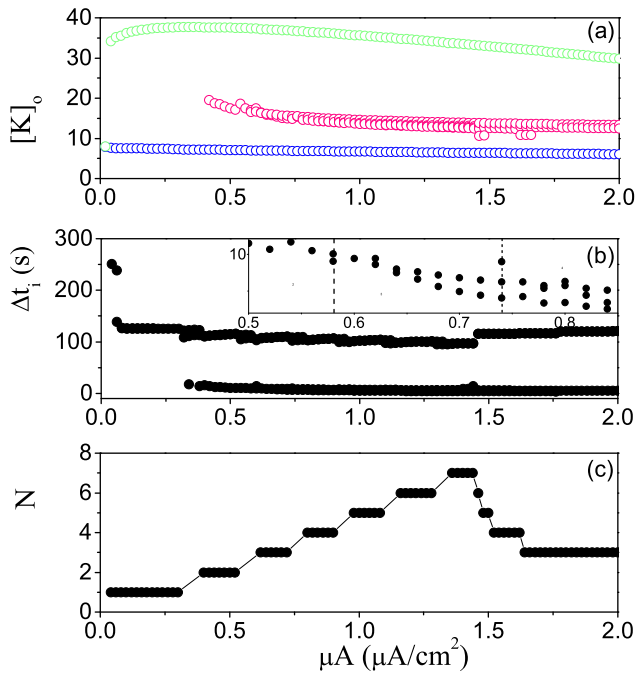


FIG. 6. (a) Bifurcation diagram of $[K]_o$ for the maximal (green circles), local maximal (pink circles), and minimal (blue circles) values. (b) The bifurcation of Δt_i (the time interval of successive $[K]_o$ spikes). The inset of (b) gives a zoomed-in part of (b) showing a variety of transitions. (c) The number of bursts N against AC injection amplitude A , indicating the $N \rightarrow N + 1$ bifurcation. $\omega = 0.008$ Hz, $[O_2] = 30.0$ mg/l, and $r_c = 4.95$ μm .

of alternating current $A \cos 2\pi\omega t$ with an angular frequency $\omega = 0.008$ Hz on the spiking patterns. In this section, we fix the cell's radius $r_c = 4.95$ μm where the cell is in steady state without stimulus. Figures 6(a) and 6(b) show the maximal, second largest, and minimal values of $[K]_o$ against the amplitude A of AC stimulus, and also the bifurcation of Δt_i ,

which is defined as the inter-spike interval of $[K]_o$ [as shown in Fig. 7(b)], respectively. For the various amplitudes of the electrical stimulus, $[K]_o$ has different oscillation modes. For the weak stimulus ($A < 0.04$ $\mu A/cm^2$), $[K]_o$ oscillates around 8.0 mM with a very small amplitude (not shown). $[K]_o$ oscillates with a large amplitude and period if the amplitude A becomes larger than 0.04 $\mu A/cm^2$. The peak of potassium concentration is over 30.0 mM and the inter-spike interval $\Delta t_i > 100$ s. $[K]_o$ accumulation with a large amplitude leads to the periodic SD state [Fig. 7(a)]. Interestingly, the second peak of $[K]_o$ ($[K]_o < 20$ mM) shows up after the largest peak appeared as the AC amplitude is over 0.32 $\mu A/cm^2$ [Fig. 7(b)], which induces the mixed state with one SZ ($[K]_o < 20$ mM) and one SD ($[K]_o > 20$ mM) state [Fig. 7(b)]. We also find that the third or fourth peak of $[K]_o$ appears with an increase in A , and the mixed state with one SD state and many SZ states is observed clearly, as shown in Figs. 7(c) and 7(d). Three or four different intervals can also be found from the zoomed-in part of Fig. 6(b). From the time series of V in one period, Fig. 7 shows clearly the change in the number of bursts with an increase in A . The number of bursts N against A is shown in Fig. 6(c) in which the period $N \rightarrow$ period $N + 1$ bifurcation is observed clearly.

Our simulation results show that the cell has a different response to the external stimulus with a faster frequency, such as at $\omega = 0.477$ Hz. Figure 8(a) gives a bifurcation of the maximal, second largest, and minimal values of $[K]_o$. For $A < 0.1$ $\mu A/cm^2$, $[K]_o$ oscillates with a very small amplitude. There is a sudden increase in the amplitude of $[K]_o$ if the amplitude of stimulus A is over 0.1 $\mu A/cm^2$. The peak of $[K]_o$ is over 35 mM, and the neuron exhibits the periodic SD state. The second peak of $[K]_o$ ($[K]_o < 20$ mM) occurs when we increase A over 0.64 $\mu A/cm^2$ [Fig. 8(a)]. However, the small peak of $[K]_o$ is in front of the large one, which leads to a

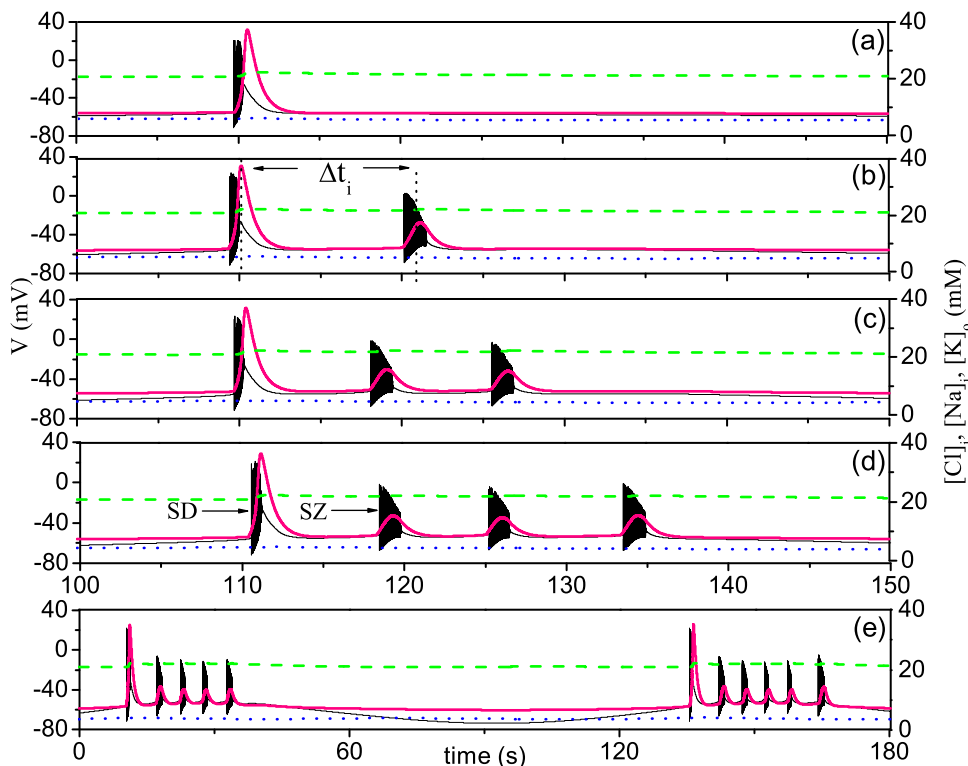


FIG. 7. [(a)–(e)] Time series of V (black lines), $[K]_o$ (pink lines), $[Na]_i$ (green lines), and $[Cl]_i$ (blue lines) for AC injection amplitude $A = 0.2$ $\mu A/cm^2$, giving a single SD event (a), 0.5 $\mu A/cm^2$, giving a mixed state with a SD burst followed by one SZ burst (b), 0.7 $\mu A/cm^2$, giving a mixed state with a SD burst followed by two SZ bursts (c), 0.9 $\mu A/cm^2$, giving a mixed state with a SD burst followed by three SZ bursts (d), and 1.1 $\mu A/cm^2$, giving a complex oscillation behavior (e). Here, $\omega = 0.008$ Hz, $[O_2] = 30.0$ mg/l, and $r_c = 4.95$ μm .

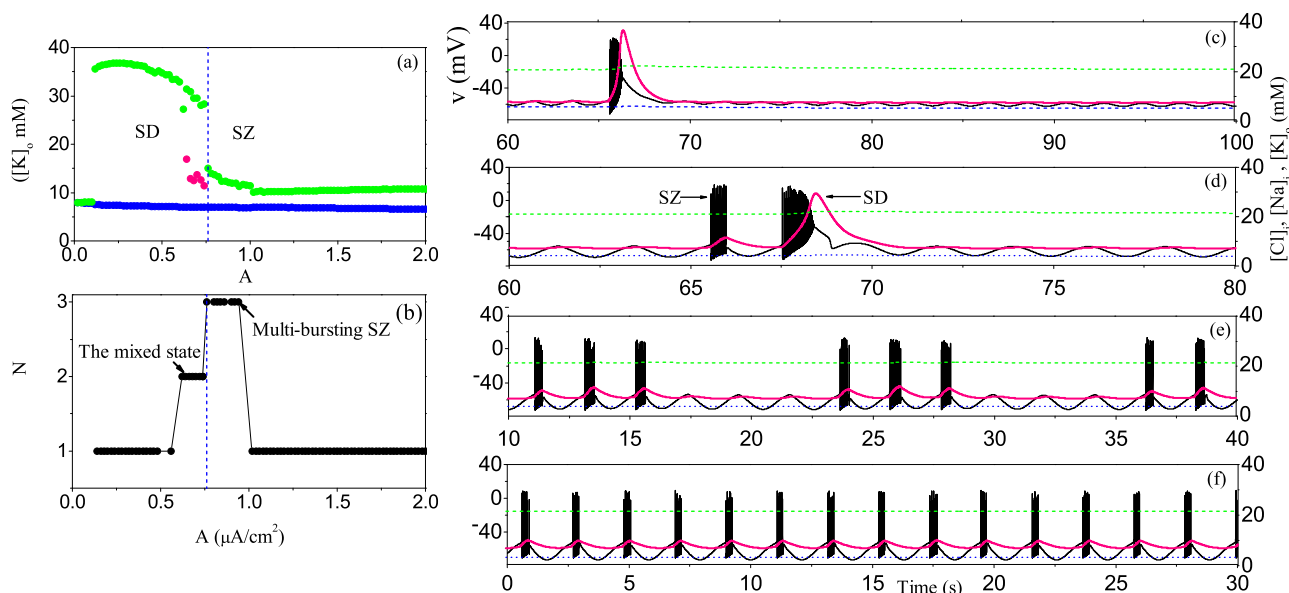


FIG. 8. (a) Bifurcation diagram of $[K]_0$ for the maximal (green circles), local maximal (pink circles), and minimal (blue circles) values. (b) The number of bursts N against AC injection amplitude A . (c)–(f) Example time series of V (black lines), $[K]_0$ (pink lines), $[Na]_i$ (green lines), and $[Cl]_i$ (blue lines) in one period for $A = 0.2 \mu\text{A}/\text{cm}^2$, giving a single SD event (c), $0.7 \mu\text{A}/\text{cm}^2$, giving a mixed state with a SZ state followed by a SD state (d), $0.9 \mu\text{A}/\text{cm}^2$, giving a multi-burst SZ state (e), and $1.1 \mu\text{A}/\text{cm}^2$, giving a single SZ event (f). $\omega = 0.477$ Hz, $[O_2] = 30.0$ mg/l, and $\tau_c = 4.95 \mu\text{m}$.

different mixed state of single SZ and SD bursts, as shown in Fig. 8(d). When A increases over $0.76 \mu\text{A}/\text{cm}^2$, the maximal concentration of potassium decreases suddenly below 15 mM [Fig. 8(a)], and the mixed state transforms to a SZ behavior [Fig. 8(f)]. Interestingly, there are two different SZ states, the multi-burst and single burst SZ states. There are many bursts in one period for the multi-burst SZ state, which is shown clearly in Fig. 8(e). The period-adding bifurcation is also observed by counting the number of bursts, as shown in Fig. 8(b).

Finally, the dynamical phase diagrams are plotted in Figs. 9(a) and 9(b) on the $([O_2], A)$ plane for different angular frequency $\omega = 0.008$ Hz and 0.477 Hz, respectively. The cell exhibits six primary features: SD state, SZ state, mixed state, SZ state with many bursts (Multi-SZ), non-excitation state (NE), and complex oscillation (CO). The NE state corresponds to the gray region which does not show any activity with the stimulus. Complex oscillation is shown in Fig. 7(e) and is marked by white dots. We found that the cell will be

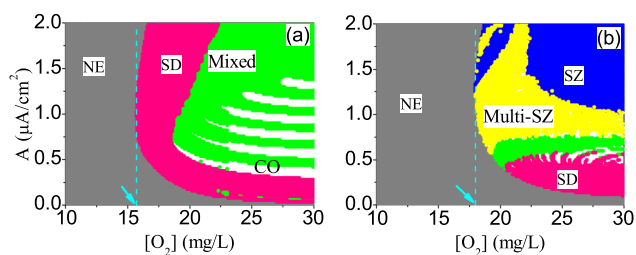


FIG. 9. [(a) and (b)] Phase diagram on the $([O_2], A)$ plane for different dynamical regions with $\omega = 0.008$ Hz and 0.477 Hz, respectively. The letters SD, SZ, Mixed, Multi-SZ, and CO stand for the spreading depression, seizure, mixed state, seizure with many bursts in one period, and complex oscillation, respectively. The letter NE stands for non-exciting state where the potential of neuron oscillates around the steady state. The white region corresponds to the complex oscillation (CO). The mixed state is determined by the maximal value of $[K]_0 > 20$ mM and the second peak value.

excited by alternating current when the oxygen concentration is over the critical values, i.e., $[O_2]_c = 15.7$ mg/l and 18 mg/l for $\omega = 0.008$ Hz and 0.477 Hz, respectively.

IV. CONCLUSIONS AND DISCUSSIONS

In our work, the effect of current stimulus on the dynamics of seizure and spreading depression was investigated systematically using a biologically realistic neuron model in which various fixed oxygen concentrations and the dynamically evolving potassium, sodium, and chloride concentrations are considered. Our numerical results reveal that rich patterns of spiking activity can be induced by the different $[K]_0$ accumulations due to current stimulus. The alternating current stimulus can produce, epileptic seizure (SZ) and spreading depression (SD) states, two different mixed states (the mixed state of SD with many SZ states and the mixed state of one SZ followed by one SD state), and the multi-SZ state which contains many SZ bursts. The direct current stimulus can also induce rich dynamical behaviors, including two different types of SZ state and SD states. In addition, we discovered that $[K]_0$ decreases continuously (or discontinuously) with increasing strength of current I , involving second (or first) phase transition according to the theory of phase transition which accounts for the different electrical activities observed.

The stimulus-induced oscillations play an important role in a variety of brain operations.^{45–47} Various neuronal firing patterns responding to external stimulus have been investigated experimentally and theoretically.^{48–51} Furthermore, the stimuli have a close relationship with neuropathic disease.⁵² The treatment or control of epileptic seizure by using stimulus perturbations provides a valuable method which may replace anti-epileptic drugs, which has been investigated experimentally in both animal^{53,54} and human^{55,56} models. Although the

design of a realizable and efficient stimulus scheme requires knowledge of the underlying mechanisms of the generation of seizures, mathematical models can provide an effective method to reveal these mechanisms and test the potential effects of different stimuli before their application in patients. Our model is simple, but it is successful in producing the behaviors of seizure and spreading depression observed in experiment.⁵⁷ In the paper by Hubel *et al.*,⁵⁸ the neuron model is based on the Hodgkin-Huxley (HH) formalism and the effect of the current of the ion pump on the spiking dynamics. Rich bifurcation behaviors such as bistability have been found in the system with the variation of the maximal pump rate. In our study, we employ a non-ionic driving current, either a direct or alternating current, for stimulus on the neuronal model, as considered by many researchers for HH-neuron simulation. However, it is interesting in the future to discuss the neuronal dynamics stimulated by an ionic flux current, such as an ion pump current, which may affect the shape and structure of the bifurcations of the neuron, resulting in rich dynamics.

Our work reveals that microenvironments, including the oxygen concentration, dynamically evolving ion concentrations, and the cell's size, play important roles in understanding pathological dynamics, such as epileptic seizures and spreading depression. Although we did not consider the effect of dynamics of the oxygen concentration and volume, the reduced model in our paper can also show rich spiking patterns induced by the current stimulus, even for low oxygen concentration. In addition, we found two different types of phase transition between the SD state and the SZ state via the reduced model according to phase transition theory, which is related closely to electrical activities. A more realistic model may provide deeper insight into the effects of dynamic microenvironment on neuronal activity.

ACKNOWLEDGMENTS

This work was supported by the National Natural Science Foundation of China under Grant Nos. 11675112 and 11675134, the Natural Science Foundation of Zhejiang Province under Grant No. LY16A050001, and the 111 Project under Grant No. B16029.

- ¹W. Penfield, K. von Sántha, and A. Cipriani, *J. Neurophysiol.* **2**, 257 (1939).
- ²P. Andersen, T. V. P. Bliss, and K. K. Skrede, *Exp. Brain Res.* **13**, 208 (1971).
- ³A. A. P. Leão, *J. Neurophysiol.* **7**, 359 (1944).
- ⁴M. A. Dichter, C. J. Herman, and M. Selzer, *Brain Res.* **48**, 173 (1972).
- ⁵A. P. Fetzinger and J. B. Ranck, *Exp. Neurol.* **26**, 571 (1970).
- ⁶G. Somjen, *Ann. Rev. Physiol.* **41**, 159 (1979).
- ⁷E. C. Zuckermann and G. H. Glaser, *Exp. Neurol.* **20**, 87 (1968).
- ⁸W. R. Anderson, J. A. E. Franck, W. L. Stahl, and A. A. Maki, *Epilepsy research* **17**, 221 (1994); available at <https://www.sciencedirect.com/science/article/pii/0920121194900523>.
- ⁹S. Gabriel, A. Eilers, A. Kivi, R. Kovacs, K. Schulze, T. N. Lehmann, and U. Heinemann, *Neurosci. Lett.* **242**, 9 (1998).

- ¹⁰J. Bureš, *et al.*, *An. Acad. Bras. Cienc.* **56**, 385 (1984); available at <https://europepmc.org/abstract/med/6099987> and <https://www.ncbi.nlm.nih.gov/pubmed/6099987#>.
- ¹¹U. Heinemann and H. D. Lux, *Brain Res.* **120**, 231 (1977).
- ¹²C. Nicholson, *An. Acad. Bras. Cienc.* **56**, 481 (1984); available at <https://europepmc.org/abstract/med/6398639> and <https://www.ncbi.nlm.nih.gov/pubmed/6398639>.
- ¹³H. Kager, W. J. Wadman, and G. G. Somjen, *J. Neurophysiol.* **84**, 495 (2000).
- ¹⁴I. Dietzel, U. Heinemann, G. Hofmeier, and H. D. Lux, *Exp. Brain Res.* **40**, 432 (1980).
- ¹⁵B. Frankenhaeuser and A. L. Hodgkin, *J. Physiol.* **131**, 341 (1956).
- ¹⁶A. P. Fetzinger and J. B. Ranck, *Exp. Neurol.* **26**, 571 (1970).
- ¹⁷U. Heinemann, H. D. Lux, and M. J. Gutnick, *Exp. Brain Res.* **27**, 237 (1977).
- ¹⁸S. Onizuka, *et al.*, *Anesthesiology* **101**, 110 (2004).
- ¹⁹K. Raley Susman, *et al.*, *J. Neurophysiol.* **86**, 2715 (2001).
- ²⁰M. Muller and G. G. Somjen, *J. Neurophysiol.* **83**, 735 (2000).
- ²¹E. I. Ekinici, *et al.*, *Diabet. Med.* **27**, 1401 (2010).
- ²²L. Resnick, *et al.*, *Hypertension* **38**, 709 (2001).
- ²³A. Zaza, *Europace* **11**, 421 (2009).
- ²⁴G. Ullah and S. J. Schiff, *PLoS Comput. Biol.* **5**, e1000776 (2010).
- ²⁵J. R. Cressman, *et al.*, *J. Comput. Neurosci.* **26**, 159 (2009).
- ²⁶H. Kager, W. J. Wadman, and G. G. Somjen, *J. Neurophysiol.* **84**, 495 (2000).
- ²⁷E. Barreto and J. R. Cressman, *J. Biol. Phys.* **37**, 361 (2011).
- ²⁸M. Bazhenov, I. Timofeev, M. Steriade, and T. J. Sejnowski, *J. Neurophysiol.* **92**, 1116 (2004).
- ²⁹X. X. Wu and J. W. Shuai, *Phys. Rev. E* **85**, 061911 (2012).
- ³⁰G. G. Somjen, *Ions in the Brain* (Oxford University Press, New York, 2004).
- ³¹N. Hübel and G. Ullah, *PLoS One* **11**, e0147060 (2016).
- ³²N. Hübel and M. A. Dahlem, *PLoS Comput. Biol.* **10**, e1003941 (2014).
- ³³S. N. Roper, *et al.*, *Ann. Neurol.* **31**, 81 (1992).
- ³⁴R. D. Andrew, *Science* **101**, 7 (1991); available at [https://www.jns-journal.com/article/0022-510X\(91\)90013-W/pdf](https://www.jns-journal.com/article/0022-510X(91)90013-W/pdf).
- ³⁵R. W. Snow and F. E. Dudek, *Brain Res.* **323**, 114 (1984).
- ³⁶B. Hill, E. D. Schubert, M. A. Nokes, and R. P. Michelson, *Science* **196**, 426 (1977).
- ³⁷K. Iwasa, I. Tasaki, and R. C. IGibbons, *Science* **210**, 338 (1980).
- ³⁸R. D. Andrew and B. MacVicar, *Neuroscience* **62**, 371 (1994).
- ³⁹R. D. Fields, *Sci. Signal.* **4**, tr1 (2011).
- ⁴⁰G. Ullah, Y. Wei, M. A. Dahlem, M. Wechselberger, and S. J. Schiff, *PLoS Comput. Biol.* **14**, 1004414 (2015).
- ⁴¹Y. Wei, G. Ullah, and S. J. Schiff, *J. Neurosci.* **34**, 11733 (2014).
- ⁴²Y. Wei, G. Ullah, J. Ingram, and S. J. Schiff, *J. Neurophysiol.* **112**, 413 (2014).
- ⁴³T. Acker and H. Acker, *J. Exp. Biol.* **207**, 3171 (2004).
- ⁴⁴J. A. Neubauer and J. Sunderram, *Appl. Physiol.* **96**, 367 (2004).
- ⁴⁵T. Womelsdorf, *et al.*, *Science* **316**, 1609 (2007).
- ⁴⁶P. Lakatos, *et al.*, *J. Neurophysiol.* **94**, 1904 (2005).
- ⁴⁷P. Fries, *Trends Cogn. Sci.* **9**, 474 (2005).
- ⁴⁸G. Matsumoto, *et al.*, *Phys. Lett. A* **123**, 162 (1987).
- ⁴⁹N. Takahashi, Y. Hanyu, T. Musha, R. Kubo, and G. Matsumoto, *Physica D* **43**, 318 (1990).
- ⁵⁰D. T. Kaplan, *et al.*, *Phys. Rev. Lett.* **76**, 4074 (1996).
- ⁵¹W. Ren, *et al.*, *Int. J. Bifurcat. Chaos* **7**, 1867 (1997).
- ⁵²S. A. Prescott, Y. D. Koninck, and T. J. Sejnowski, *PLoS Comput. Biol.* **4**, e1000198 (2008).
- ⁵³A. Berenyi, M. Belluscio, D. Mao, and G. Buzsaki, *Science* **337**, 735 (2012).
- ⁵⁴S. Saitlet, S. Gharbi, G. Charvet, C. Deransart, R. Guillemaud, *et al.*, *Brain Stimul.* **6**, 241 (2013).
- ⁵⁵S. Dedeurwaerdere, *et al.*, *Epilepsy Res.* **59**, 191 (2004).
- ⁵⁶P. Rajna and C. Lona, *Epilepsia* **30**, 168 (1989).
- ⁵⁷J. Ingram, *et al.*, *J. Neurophysiol.* **112**, 205 (2014).
- ⁵⁸N. Hübel, E. Schöll, and M. A. Dahlem, *PLoS Comput. Biol.* **10**, e1003551 (2014).